Fusion Science and Technology

ISSN: 1536-1055 (Print) 1943-7641 (Online) Journal homepage: https://www.tandfonline.com/loi/ufst20

Modeling of Ablatant Deposition from Electromagnetically Driven Radiative Pellets for Disruption Mitigation Studies

Robert Lunsford, Roger Raman, A. Brooks, R. A. Ellis & W.-S. Lay

To cite this article: Robert Lunsford, Roger Raman, A. Brooks, R. A. Ellis & W.-S. Lay (2019) Modeling of Ablatant Deposition from Electromagnetically Driven Radiative Pellets for Disruption Mitigation Studies, Fusion Science and Technology, 75:8, 767-774, DOI: 10.1080/15361055.2019.1629246

To link to this article: https://doi.org/10.1080/15361055.2019.1629246

FUSION SCIENCE AND TECHNOLOGY · VOLUME 75 · 767–774 · NOVEMBER 2019

DOI: https://doi.org/10.1080/15361055.2019.1629246

Modeling of Ablatant Deposition from Electromagnetically Driven Radiative Pellets for Disruption Mitigation Studies

Robert Lunsford,[a]* Roger Raman,[b] A. Brooks,[a] R. A. Ellis,[a] and W.-S. Lay[b]

[a]*Princeton Plasma Physics Laboratory, Princeton, New Jersey*
[b]*University of Washington, Seattle, Washington*

Received May 18, 2018
Accepted for Publication June 5, 2019

Abstract — *The electromagnetic particle injector (EPI) concept is advanced through the simulation of ablatant deposition into ITER H-mode discharges with calculations showing penetration past the H-mode pedestal for a range of injection velocities and granule sizes concurrent with the requirements of disruption mitigation. As discharge stored energy increases in future fusion devices such as ITER, control and handling of disruption events become critical issues. An unmitigated disruption could lead to failure of the plasma-facing components resulting in financially and politically costly repairs. Methods to facilitate the quench of an unstable high-current discharge are required. With the onset warning time for some ITER disruption events estimated to be less than 10 ms, a disruption mitigation system needs to be considered that operates at injection speeds greater than gaseous sound speeds. Such an actuator could then serve as a means to augment presently planned pneumatic injection systems. The EPI uses a railgun concept whereby a radiative payload is delivered into the discharge by means of the J×B forces generated by an external current pulse, allowing for injection velocities in excess of 1 km/s. The present status of the EPI project is outlined, including the addition of boost magnetic coils. These coils augment the self-generated railgun magnetic field and thus provide a more efficient acceleration of the payload. The coils and the holder designed to constrain them have been modeled with the ANSYS code to ensure structural integrity through the range of operational coil currents.*

Keywords — *Disruption mitigation, railgun, pellet, neutral gas shielding.*

Note — *Some figures may be in color only in the electronic version.*

I. INTRODUCTION

Mitigation of disruption events is a critical need for ITER as well as any other future burning plasma device. Disruptions can lead to reduced component lifetime and possible first-wall failure due to damages incurred through impact of relativistic electrons, extreme localized heating, and large electromechanical forces.[1] Present disruption mitigation strategies involve the rapid injection of large quantities of impurities ensuring that the resultant thermal quench is dominated by radiative rather than conductive heat losses. In order to provide sufficient preemptive mitigation of the disruption event, the radiative payload must be delivered to the discharge with a warning time that could be as small as 10 ms (Ref. 2). In addition, for the mitigation strategy to be maximally effective, the impurity source must rapidly penetrate the H-mode transport barrier to concentrate deposition within the core of the discharge. As discharge stored energy and confinement increase, these timescale and penetration requirements challenge the response of presently employed disruption mitigation strategies.[3–5]

To address these issues, the electromagnetic injection of a dense solid projectile containing a radiative payload is proposed as a disruption mitigation system (DMS). The electromagnetic particle injector[6] (EPI) is based upon a railgun concept whereby current driven through a metallic spring connecting conducting rails in the presence of an eternally applied magnetic field generates

*E-mail: rlunsfor@pppl.gov

a $J \times B$ acceleration. The EPI has demonstrated the ability to accelerate a projectile to 150 m/s with a 1.0-ms response time, consistent with baseline calculations.[7] While the EPI has yet to be used for injection into a discharge, prior injection experiments[8] have shown that the radiative payload begins to ablate upon reaching the steep gradient region of the plasma edge, generating a field-aligned plume of ionized material as it transits the discharge. This described scenario is based on prior injection experiments[8] with smaller radiative granules. These experiments have shown neutral gas shielding simulations of ablation rates for boron nitride (BN) pellets injected into ITER baseline discharges as described in Sec. III, have provided particle deposition profiles, and have shown that the depositional barycenter of the injected pellet occurs within the core of the discharge thus providing a localized impurity source that rapidly stimulates a controlled radiative collapse.

II. EPI ASSEMBLY

The basic components of the railgun system are shown in Fig. 1. A current is passed between the pair of conducting rails by means of a curved metallic spring called a sabot. In a standard railgun configuration, a rapidly triggered capacitor bank connected to the back of the rails drives a current pulse through the rails and sabot. The loop current generates a magnetic field B_{RG}, which interacts with the current passing through the sabot to create a $J \times B_{RG}$ force driving the sabot forward and accelerating the payload along the rails. At the end of the rails is a catch mechanism that arrests the sabot and allows the radiative payload to continue into the discharge unencumbered.

To accelerate the sabot to injection velocities over the rail length (~1 m), the energy density deposited within it must by necessity be large, which can result in a loss of structural rigidity for the rail and sabot system. In addition, at highly driven currents, the rail electrode erosion can be substantial, thus limiting the lifetime between electrode refurbishment. However, as the acceleration is the product of the current and magnetic field, these issues can be overcome by implementing supplemental high field magnetic coils on either side of the delivery rail electrodes thus augmenting the railgun-generated magnetic fields. These additional coils improve system efficiency while reducing the energy deposited into the sabot. In addition, these fields serendipitously mimic the fringing magnetic fields that exist adjacent to fusion research tokamaks.

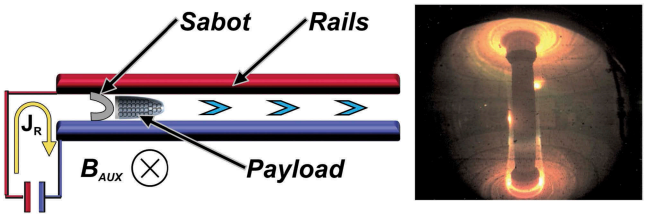

Fig. 1. Components of the EPI railgun system. Direction of travel is indicated by the chevrons and the representative plasma discharge on the figure's right side.

To test the efficacy of the supplemental magnetic field concept, a set of 40 turn American wire gauge 5 copper coils has been built and positioned directly above and below the EPI rails. The forces on the coils due to the firing currents are borne by an external set of coil supports as shown in Fig. 2. In the present design, stainless steel bars ["B)"] with a 2-in. cross section are connected at the end with G10 nonconducting transverse support ["C)"] end pieces to minimize current loops. The cross straps are made of 0.125-in.-thick titanium bars, press fit onto titanium pins to carry the majority of the expansive load. Individual coil assemblies have been tested at up to 6.2-kA coil current resulting in magnetic fields between the coils of nearly 2 T. This prototype has been also tested in the full railgun assembly, with both coils operated in series using a single 10-mF, 1.5-kV power supply. A coil current of 4.2 kA resulted in 1.3 T of boost field generated at the railgun location concurrent with the railgun firing. At present, the coils are limited by the available power supplies, and operation of the full assembly at 2-T fields between the rails is planned after the power supplies are upgraded in the near future.

Achieving the desired design criterion of a 3-T boost field requires a 10-kA coil current. To account for the increased load, we have calculated the stresses resultant on the coil holder and modified the design to utilize the more robust Inconel 625 for the mainline supports with transverse support straps and pins made of Inconel 718. The thickness of the straps is also increased to 0.375 in. The results of the simulated loads using the ANSYS analysis code package are shown in Fig. 3. As is seen, the forces on the support structures are within the material stress limits with a stress concentration at the retaining pin of 696 MPa, which is sufficiently below the 825-MPa limit set by a 1.5× safety margin.

III. SIMULATED INJECTIONS INTO ITER BASELINE DISCHARGES

In order to model the depositional profiles of the injected pellets, we utilized an adaptation of a spherically symmetric neutral gas shielding model for injection of

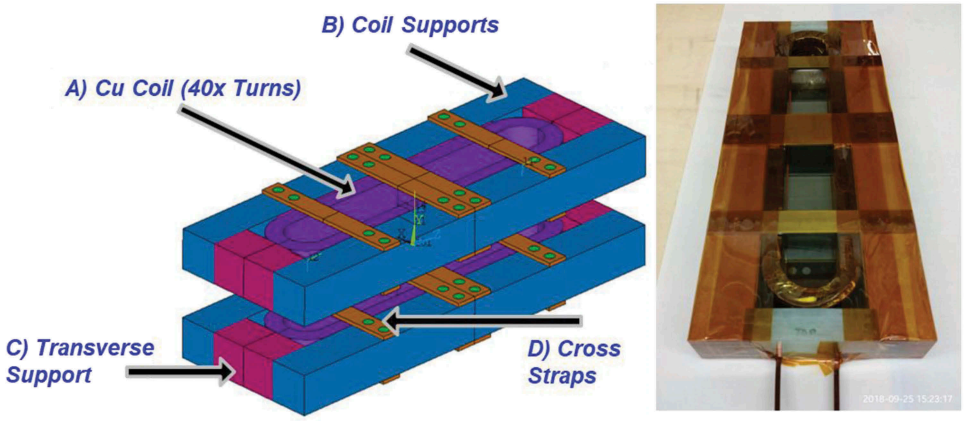

Fig. 2. Supplemental boost coil and supporting coil holder assembly drawing and picture. For the initial prototype testing, the coil supports "B)" are made of stainless steel while the transverse supports are insulating G-10. The cross straps are 3/8-in. titanium bars held in place with press fit titanium pins (green circles). The lines across the center of the transverse supports and cross straps are simply indicative of an axis of symmetry and do not represent a physical split in the material.

light refractive elements as developed by Parks et al.[9] This model has been validated by comparing calculations to sub-millimeter lithium granule injection experiments on the Experimental Advanced Superconducting Tokamak[8] (EAST) as well as lithium,[10] carbon, and boron carbide[11,12] injections on DIII-D. In this model, as the outer layers of the injected pellet are ablated, a dense neutral cloud is formed around the pellet that then moderates the incoming heat flux allowing the pellet to penetrate more deeply into the discharge. Further descriptions of the model can be found in Refs. 9, 13, 14, and 15. The extent to which the intervening neutral cloud modulates the income heat flux is contained within the shielding parameter η as seen in Eq. (1), where the change in granule radius is proportional to the heat flux q_s and the combined electrostatic shielding and field-directed heating anisotropy f_H and is inversely proportional to the granule density n_g, sublimation energy ΔH_g, and surface temperature T_s:

$$\frac{dr_g}{dt} = q_s \times f_H \frac{\eta}{n_g\left(\Delta H_g + {}^{10}/_{3}T_s\right)} . \tag{1}$$

The experimentally determined shielding parameter varies between zero and one, where zero is an indication of complete shielding of the pellet and larger numbers represent a greater penetration of the incident heat flux, and thus a lesser shielding fraction. The heat flux to the granule q_s is described by Eq. (2):

$$q_s = {}^{1}/_{2} n_e T_e \left(\frac{8T_e}{\pi m_e}\right)^{1/2}, \tag{2}$$

where

m_e = electron mass

n_e = plasma electron density

T_e = electron temperature.

For the majority of these simulations, we model the injection of a solid spherical BN pellet. Boron nitride was chosen due to the well-understood radiative properties of the contained nitrogen and its compatibility as a material of choice for present-day tokomaks. Returning to Eq. (1), the density of cubic BN is 8.37×10^{28} atoms/m^3, and the surface temperature is assumed to be the vaporization temperature of the material, namely, 3246 K (0.28 eV). The sublimation energy was determined to be between 30 and 35 MJ/kg through heat flux measurements to bulk material,[16] and the average value has been converted to 8.36 eV/atom for use in this simulation. The pellets were simulated as a single spherical mass driven into the midplane low field side of ITER baseline $Q = 10$ discharges as described in Ref 17 and shown in Fig. 4.

To determine the effect of parametric variations on the depositional profile, we completed three computational scans over the η, r_g, and v_{inj} (pellet injection velocity) parameters. The shielding provided by the neutral cloud is species dependent and can be affected by the heating scheme of the discharge. Specifically, granule ablation can be accelerated by superthermal ions as a result of intense neutral beam injection. As a result, it is illustrative to examine the range of deposition profiles

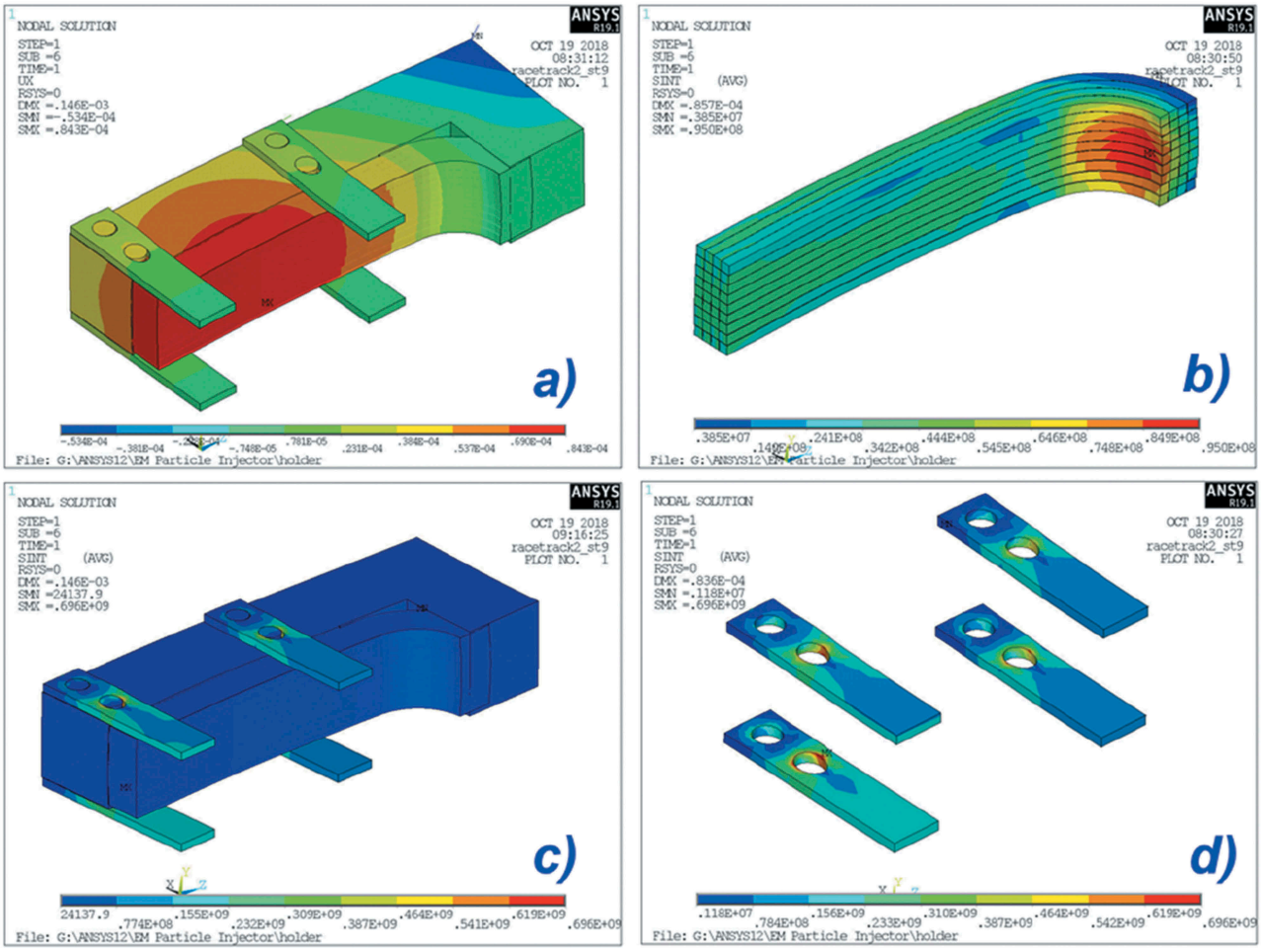

Fig. 3. ANSYS modeling of resultant stresses from 10-kA boost coil current. Since the coil is symmetric about two axes, only the upper left quadrant of all sections is shown. (a) The largest displacement occurs in the center of the support beam with a maximum deflection of 50 μm. (b) The largest stresses in the copper coil are 95-MPa Tresca stresses due to this coil deflection. (c) and (d) The majority of the stress load is being taken by the cross straps, and it is concentrated at the inner hole with a peak value of 696 MPa.

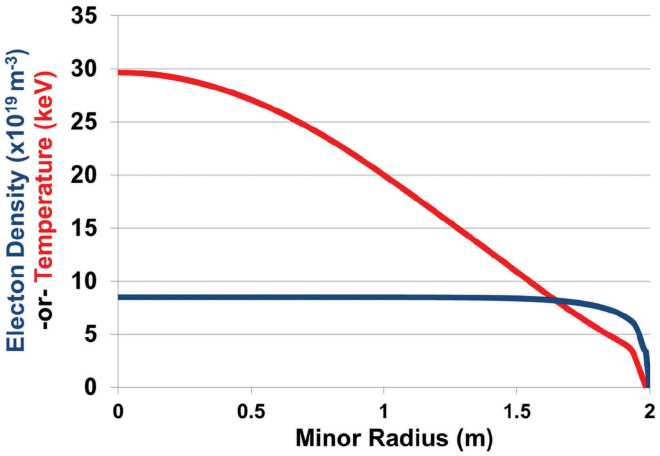

Fig. 4. Electron density and temperature for ITER $Q = 10$ high-performance H-mode scenarios as described in Ref. 17.

expected for granule injection at a range of different shielding parameters.

For this scan, shown in Fig. 5, we start the shielding parameter scan at 0.4, the average η value determined for vitreous carbon injections into DIII-D. Carbon granules share a similar Mohs hardness with BN, as well as similar sublimation temperature, although carbon does have a slightly lower sublimation energy per atom. As lower sublimation energies tend to lead to a more effective shielding of the granule (cryogenic pellets have been found to have shielding factors much closer to zero), we anticipate that this granule shielding value found for carbon granule injection represents the lowest possible value that could a priori be expected for BN pellet injection. The scan was then run up to $\eta = 1$, which is a condition whereby there is no shielding of the incoming heat flux. As can be observed,

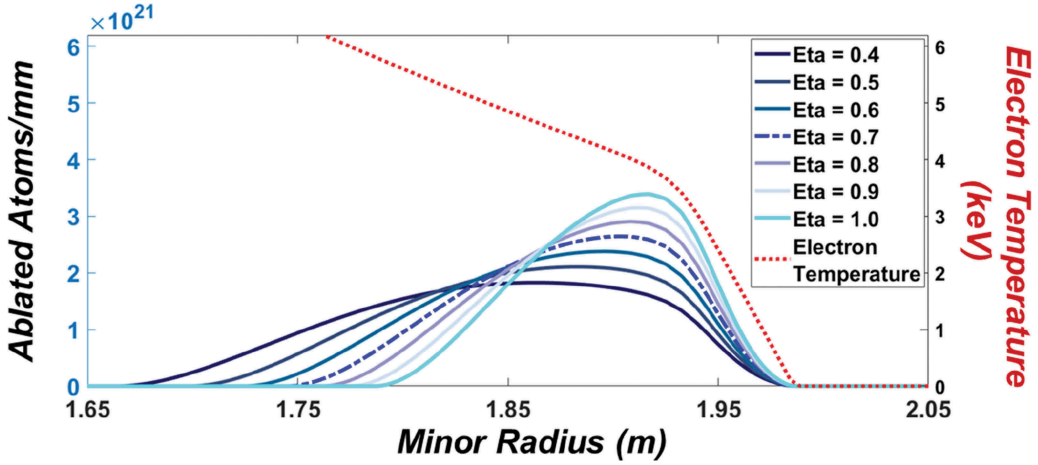

Fig. 5. Pellet ablatant deposition dependence on shielding factor for a 2-mm granule injected at 1000 m/s. Varying the pellet shielding factor from 0.4 (strong shielding) to 1.0 (no shielding) delimits the envelope for expected direct pellet deposition of radiative material. Note that over the entire shielding range, the granule is able to penetrate the pedestal region and deposit substantial mass into the discharge core. The temperature plot is included to indicate the location of the discharge profile.

the addition of the increased shielding moves the farthest extent of the deposition profile inboard by 10 cm. We anticipate the extent of the pellet self-shielding to lie somewhere between these two extremes and thus adopt a shielding factor of 0.7 (dashed line in Fig. 5) for the remaining simulations.

Variations in granule size will also affect the penetration of the granules as is evidenced in Fig. 6. As anticipated, larger granules deposit a greater amount of material farther into the discharge. However, it is important to note that in all cases the granules are fully ablated prior to reaching the magnetic axis, and while these simulations do not take into account immediate cooling of the discharge due to ablatant deposition, this result or early full ablation moderates concerns of a solid pellet interacting with a material surface.

These simulations can be used to provide an initial material deposition profile for magnetohydrodynamic disruption simulation codes such as JOREK and NIMROD to determine the material quantity required to generate a radiative collapse in ITER. Using a nominal shielding value of $\eta = 0.7$ and a midrange granule radius of 2 cm, we calculate the mass injection profile for a range of velocities from 100 to 2000 m/s. These results are displayed in the intensity plot in Fig. 7. As can be seen, the mass deposition profile shifts sharply inward as

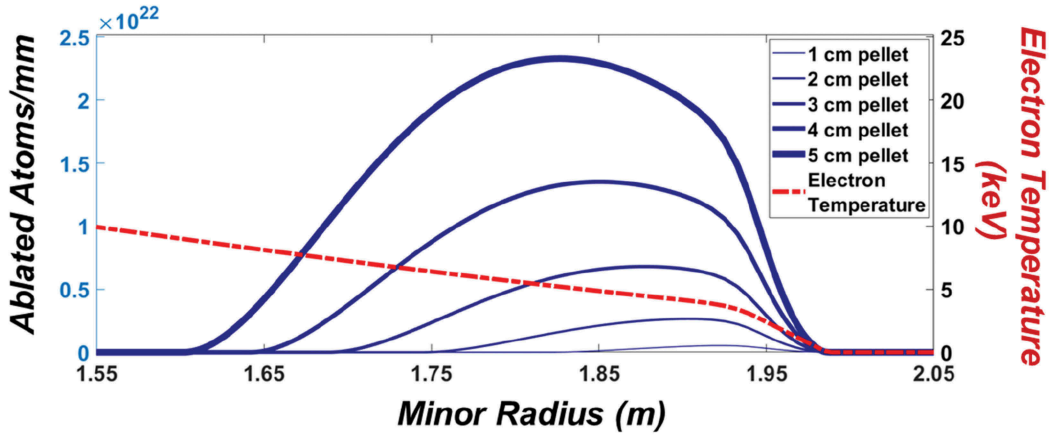

Fig. 6. Ablatant deposition for a range of granule sizes injected at 1000 m/s with an assumed $\eta = 0.7$. We note two results from this simulation scan. First, all but the smallest granule sizes are able deposit the majority of their mass into the discharge core. Second, even for the largest-sized granules, there is full ablation well before the magnetic axis, thus reducing the likelihood that an injected granule will impact a material surface. The temperature plot is included to indicate the location of the discharge profile.

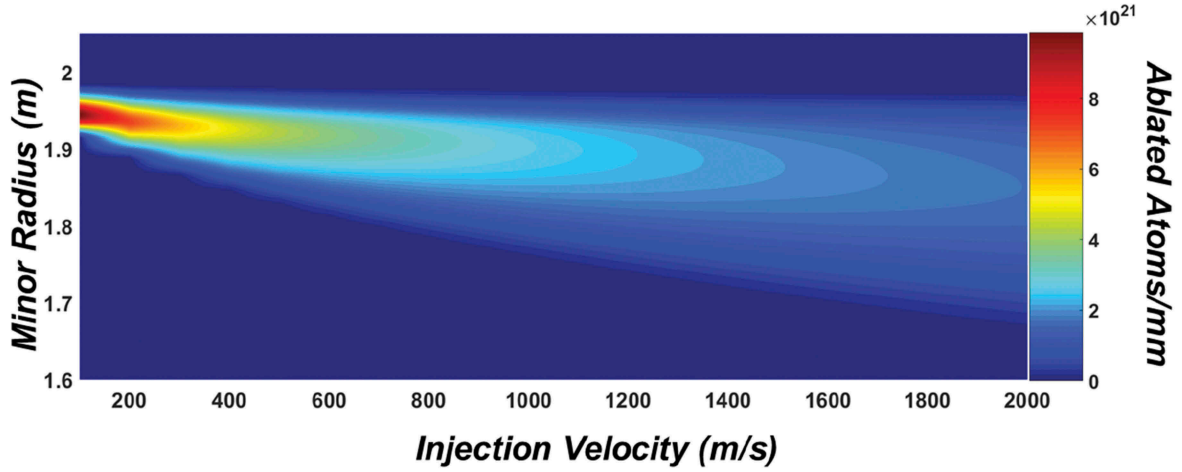

Fig. 7. Injection deposition profile at extended range of injection velocities for a 2-cm pellet with an assumed $\eta = 0.7$. The ability of the EPI to tune the deposition location of the injected mass through a variation in injection velocities by a simple scaling in railgun current is a unique feature of this actuator type.

the velocity is increased. Operationally, this value is completely determinable from the settings on the EPI and can be tuned for maximum effectiveness during the course of the research program.

In addition, the EPI is capable of injecting either a solid pellet or a shell pellet containing a collection of smaller ablative spheres. A cluster of smaller pellets is projected to ablate more rapidly than a single large pellet due to its larger collective surface area. Figure 8 shows the results of a filled shell pellet injection. In this simulation a pair of 5-cm BN pellets with walls of 1-cm thickness and 0.5-cm thickness is injected at 500 m/s into the discharge edge, with the lower velocity being chosen to shift the depositional profile outboard. The internal volume of the shell is filled with 500-μm-diameter solid BN spheres. Assuming a loose packing fraction of 0.6, this is approximately 130 000 BN granules for the thick shell and 330 000 for the thin shell. The simulation assumes that the ablation of the shell is spherically symmetric and that it leads to a neutral shielding cloud that is still maintained allowing uniform collisional heating of the microspheres after the outer shell degradation.

As the simulation shows (Fig. 8), the ablations progress as before during the initial injection period right up until the point where the outer shell is completely ablated. This occurs at a minor radial location of 1.82 m for the thick shell and 1.87 m for the thin shell. At this point the ablation rate quickly increases due to the increased surface area of the microspheres, and as shown, the full internal volume of material is deposited within a few millimeters. Note that the vertical axis of Fig. 8 has been changed to a log scale to accommodate the fact that there is an order of magnitude more material deposited in a short radial distance. It is possible that this injected pellet stream will cause a localized cooling wave that could extend the deposition region. In addition this localized cooling location could also be used to rapidly reduce the pedestal temperature possibly allowing greater penetration for a high-Z cryogenic pellet or radiative gas injection. Further research with a more comprehensive code suite, benchmarked by the simultaneous injection of ablative micropellets to determine the localized pellet cooling effect, should provide a better answer and will be the focus of future research.

IV. ITER IMPLEMENTATION OF THE EPI CONCEPT

Extrapolation from the present status of the EPI program to the requirements of an ITER-class DMS begins with two initial considerations. First, does the technology scale to a system whereby an appropriately sized projectile can be injected into ITER within the relevant time window? Second, is there a strategy that allows for the implementation of such a system into an already mature ITER design without resulting in major redesigns or delays?

In answer to the first question, we note the railgun is a mature mass acceleration concept with the first instances of the utilization of electromagnetic forces to propel matter being evidenced during the early 20th century. In addition, the engineering demands of the ITER-class DMS are not beyond present engineering with the U.S. NAVSEA railgun developed in conjunction with BAE Systems having demonstrated the ability to

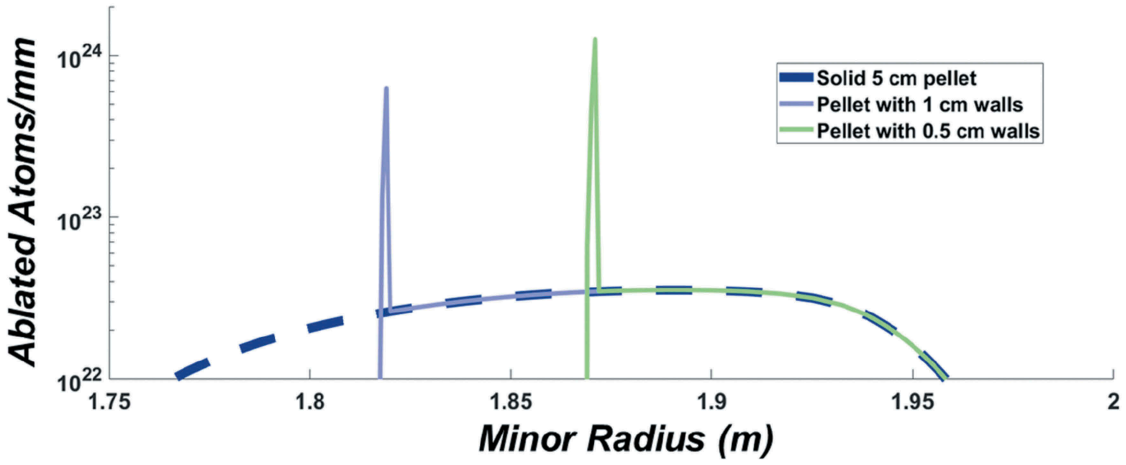

Fig. 8. Injection of a filled shell pellet at 500 m/s. In these simulations, a hollow pellet is filled with 500-μm spherical BN granules with a packing fraction of 0.6. This amounts to 130 000 granules for a shell thickness of 1 cm and 330 000 granules for a shell thickness of 0.5 cm. The simulation assumes that once the outer shell has been removed, the granules disperse and immediately begin to ablate. These are compared to the ablatant deposition of a standard solid pellet. Note that the vertical axis is now on a log scale to accommodate the range in depositional profiles.

deliver a 16-kg projectile at approximately 2000 m/s (Ref. 18). As such, while scaling of the present iteration of the EPI to an ITER-class system does present technical challenges, there are no fundamental obstacles. Velocities achievable with the EPI have been calculated by solving the railgun equations for a linear geometry[7] and show that a 100-mF capacitor bank charged to 2 kV has the ability to accelerate a 15-g mass (equivalent to a 2-cm BN sphere) to 1.3 km/s in 2 ms.

Upon exiting the EPI, delivery of the payload is accomplished by having the projectile transverse a shallow bend guide tube. This tube provides a directed injection away from the ITER center stack assembly and toward a tungsten strike plate on the opposite side of the vacuum vessel ensuring that if the DMS is actuated during a period without an active discharge, then the BN pellet will be safely arrested without impact to any of the more fragile interior components.

Incorporating the EPI system into the ITER DMS systems can be handled in one of two ways. If possible, integrating the EPI into an ITER midplane port plug allows reduced response times and greater utilization of the fringing field. However, it carries with it additional handling and maintenance challenges and as such would need to be mounted on rails to allow removal to a lower-radiation area. In addition, because of the advanced state of the ITER design, it may not be possible to redesign a port plug to accommodate such a system. In such a case, the EPI would be located exterior to the port plug with purpose-built supplemental boost coils to compensate for the lower fringing field. This location adds an additional 4 m to the distance traveled, but this additional 4 ms is still within the desired design envelope for a rapid DMS.

V. CONCLUSION

The EPI rapidly drives a solid pellet deep into the core of the discharge where it ablates and radiatively cools the discharge, effectively circumventing a localized disruptive collapse that could damage the plasma-facing components. The injector is fully electromagnetic, with the lack of mechanical moving parts ensuring high reliability after long standby periods. This satisfies the demanding needs of a prompt-acting reactor DMS. In addition, close physical proximity to a next-step fusion reactor design takes advantage of the external fringing field, increasing the EPI efficiency. As shown, the ability of the EPI to vary injection velocity by a modification of railgun current and thus change the depositional profile of the ablated material is unique among DMSs and allows tuning of the actuator to best fit the needs of the associated tokamak. Future research will focus on the development and testing of the EPI with boost coils in preparation for deployment of a prototype in anticipation of preliminary experiments at an existing tokamak facility to better quantify the effects of solid pellet injection on discharge shutdown behavior and disruption mitigation.

Acknowledgments

This work is supported by U.S. Department of Energy contract numbers DE-SC0006757 and DE-AC02-09CH11466. The digital data for this paper may be found at http://arks.princeton.edu/ark:/88435/dsp018910jx38x.

ORCID

Robert Lunsford http://orcid.org/0000-0003-3588-6801

References

1. M. SUGIHARA et al., "Disruption Scenarios, Their Mitigation and Operation Window in ITER," *Nucl. Fusion*, **47**, 337 (2007); https://doi.org/10.1088/0029-5515/47/4/012.
2. M. LEHNEN et al., "Disruptions in ITER and Strategies for Their Control and Mitigation," *J. Nucl. Mater.*, **463**, 39 (2015); https://doi.org/10.1016/j.jnucmat.2014.10.075.
3. E. M. HOLLMANN et al., "Measurements of Injected Impurity Assimilation During Massive Gas Injection Experiments in DIII-D," *Nucl. Fusion*, **48**, 115007 (2008); https://doi.org/10.1088/0029-5515/48/11/115007.
4. M. LEHNEN et al., "Disruption Mitigation by Massive Gas Injection in JET," *Nucl. Fusion*, **51**, 123010 (2011); https://doi.org/10.1088/0029-5515/51/12/123010.
5. N. COMMAUX et al., "First Demonstration of Rapid Shutdown Using Neon Shattered Pellet Injection for Thermal Quench Mitigation on DIII-D," *Nucl. Fusion*, **56**, 046007 (2016); https://doi.org/10.1088/0029-5515/56/4/046007.
6. R. RAMAN et al., "Electromagnetic Particle Injector for Fast Time Response Disruption Mitigation in Tokamaks," *Nucl. Fusion*, **59**, 016021 (2019); https://doi.org/10.1088/1741-4326/aaf192.
7. R. RAMAN et al., "Fast Time Response Electromagnetic Disruption Mitigation Concept," *Fusion Sci. Technol.*, **68**, *4*, 797 (2015); https://doi.org/10.13182/FST14-916.
8. R. LUNSFORD et al., "Injected Mass Deposition Thresholds for Lithium Granule Instigated Triggering of Edge Localized Modes on EAST," *Nucl. Fusion*, **58**, 036007 (2018); https://doi.org/10.1088/1741-4326/aaa2ac.
9. P. PARKS et al., "Analysis of Low Z_a Impurity Pellet Ablation for Fusion Diagnostic Studies," *Nucl. Fusion*, **28**, 477 (1988); https://doi.org/10.1088/0029-5515/28/3/012.
10. R. LUNSFORD et al., "Lithium Granule Ablation and Penetration During ELM Pacing Experiments at DIII-D," *Fusion Eng. Des.*, **112**, 621 (2016); https://doi.org/10.1016/j.fusengdes.2016.04.041.
11. R. LUNSFORD et al., "Multi-Species Impurity Granule Injection and Mass Deposition Projections in NSTX-U Discharges," *Nucl. Fusion*, **57**, 076008 (2017); https://doi.org/10.1088/1741-4326/aa6cd3.
12. R. LUNSFORD et al., "Supplemental ELM Control in ITER Through Beryllium Granule Injection," *Nucl. Mater. Energy*, **19**, 34 (2019); https://doi.org/10.1016/j.nme.2019.02.005.
13. G. KOCSIS et al., "On the Fluctuation of Line Radiation Emitted During Aluminum Micro-Pellet Ablation in Magnetized Plasmas," *Plasma Phys. Control. Fusion*, **41**, 881 (1999); https://doi.org/10.1088/0741-3335/41/7/303.
14. P. B. PARKS et al., "Model of Ablation Flow near Light-Atom Pellets with Surface Boundary Conditions," *Nucl. Fusion*, **34**, *3*, 417 (1994); https://doi.org/10.1088/0029-5515/34/3/I09.
15. B. PÉGOURIÉ, "Review: Pellet Injection Experiments and Modelling," *Plasma Phys. Control. Fusion*, **49**, R87 (2007); https://doi.org/10.1088/0741-3335/49/8/R01.
16. A. F. OKUNO, "Ablative and Insulating Properties of Outgassed Boron Nitride and Boron Nitride Composite," Technical Note D-3660, National Aeronautics and Space Administration (Oct. 1966).
17. T. CASPER et al., "Development of the ITER Baseline Inductive Scenario," *Nucl. Fusion*, **54**, 013005 (2014); https://doi.org/10.1088/0029-5515/54/1/013005.
18. S. J. FREEDBERG Jr., "Navy Railgun Ramps Up in Test Shots," Breaking Defense; https://breakingdefense.com/2017/05/navy-railgun-ramps-up-in-test-shots (current as of May 18, 2018).